

THE HYBRID DISCONTINUOUS GALERKIN METHOD FOR ELLIPTIC PROBLEMS AND APPLICATIONS IN VERTICAL OCEAN-SLICE MODELING

DANALIE AZOFEIFA, MIGUEL ANGEL MORELES, FEDERICO ANGEL VELAZQUEZ-MUÑOZ

ABSTRACT. Classical numerical solutions of the Navier-Stokes equations applied to Coastal Ocean Modeling are based on the Finite Volume Method and the Finite Element Method. The Finite Volume Method guarantees local and global mass conservation. A property not satisfied by the Finite Volume Method. On the down side, the Finite Volume Method requires non trivial modifications to attain high order approximations unlike the Finite Volume Method. It has been contended that the Discontinuous Galerkin Method, locally conservative and high order, is a natural progression for Coastal Ocean Modeling. Consequently, as a primer we consider the vertical ocean-slice model with the inclusion of density effects. To solve these non steady Partial Differential Equations, we develop a pressure projection method for solution. We propose a Hybridized Discontinuous Galerkin solution for the required Poisson Problem in each time step. The purpose, is to reduce the computational cost of classical applications of the Discontinuous Galerkin method. The Hybridized Discontinuous Galerkin method is first presented as a general elliptic problem solver. It is shown that a high order implementation yields fast and accurate approximations on coarse meshes.

CONTENTS

1. Introduction	2
2. Materials and Methods	3
2.1. A HDG scheme for elliptic equations	3
2.2. A pressure projection method with HDG Poisson solver	7
3. Tidal simulation in semienclosed basin	8
3.1. A Rectangular Channel	8
3.2. A Sector Channel	11
4. Vertical ocean-slice nonhydrostatic models	13
4.1. Surface Standing Waves in a Deep Basin	14
4.2. Density driven flow	16
5. Conclusions	18
References	21

1. INTRODUCTION

The numerical solution of the Navier-Stokes equations applied to Coastal Ocean Modeling (COM), is an active line of research. In Chen et al. [3], a Finite Volume Method (FVM) for COM, referred as FVCOM is proposed and compared with finite difference (FD) models. Then an extension to include non-hydrostatic effects is presented in Lai et al [8].

A motivation to develop FVCOM is the difficulty of dealing with irregular coastal geometries with FD, FVCOM applies naturally. Also, FVM guarantees local and global mass conservation. A property not satisfied by the very popular Finite Element Method (FEM). On the down side, the FVM requires non trivial modifications to attain high order approximations, unlike the FEM. Consequently, the next generation of COM is by means of methods that are locally conservative and high order. A natural choice is the Discontinuous Galerkin Method, Chen et al. [3]: *Application of these methods to current finite element coastal ocean models could significantly improve computational accuracy and efficiency as well as mass conservation.* These applications are under development, and there is an increasing literature on the subject. See Kärnä et al [7] and Pan et al [9]. In the latter a non-hydrostatic extensions to a discontinuous finite element coastal ocean model is developed.

A drawback of DG methods is that in general it is more expensive than existing numerical methods, because DG methods have many more (coupled) unknowns. A recent solution is to introduce hybridizable (hybridized) Discontinuous Galerkin Methods (HDG). The number of coupled unknowns is reduced, while retaining the attractive properties of the DG method, Tanh [2].

Consequently, the purpose of our research, it to develop the HDG in the context of COM. Of particular interest are applications to non-hydrostatic modeling. As a primer, we consider the vertical ocean-slice model with the inclusion of density effects, Kämpf [6], Lai et al. [8]. To solve these non steady PDE equations, we develop a pressure projection (PP) method for solution, see Almgren et al [1]. It is well known that these PP methods require a Poisson solver in each time step, and we propose a HDG solution. Noteworthy, HDG methods do not require penalization unlike classical DG solutions for elliptic problems, see Riviere [11]. Our implementations favor high order approximations, an attractive feature of DG methods. We do not aim for generality, comparisons with FVCOM are carried out only on rectangular meshes. It will become apparent that the application to more general meshes is straightforward.

The outline is as follows. In the Materials and Methods section, we develop an HDG scheme for the diffusion-advection-reaction equation. A distinctive step is to reduce the equation to a first order hyperbolic system. We introduce an alternative to that of Bui-Thanh [2]. Also a PP method is developed for 2D vertical-slice modeling. We stress the use of the HDG solver of the underlying Poisson problem. In Section 3 we consider pure elliptic problems in COM, namely tidal simulation

in a semienclosed basin with tidal forcing at the open boundary. Near resonance cases are considered. In Section 4 we address deep-water (short) surface gravity waves and density-driven currents, as vertical ocean-slice nonhydrostatic models. Our findings and reflections on future work, are summarized in the Conclusions section.

2. MATERIALS AND METHODS

2.1. A HDG scheme for elliptic equations. Let us consider the diffusion-advection-reaction equation for the unknown function p ,

$$(1) \quad -\nabla \cdot (\mathbf{K}\nabla p) + \beta \cdot \nabla p + cp = f.$$

It is assumed that the equation is of (strict) elliptic type, namely, the matrix function \mathbf{K} is symmetric and positive definite in its domain of definition.

Since the basic construction of the DG scheme is local, boundary conditions for well posedness shall be introduced in the corresponding step of the construction.

2.1.1. Function spaces. Assume a domain $\Omega \subset \mathbb{R}^d$ partitioned into non-overlapping elements I_j , $j = 1, \dots, N$. Let I be one of such elements. The boundary of I , ∂I is the union of uniquely defined faces e with outward pointing normal \mathbf{n} . The skeleton of the mesh, denoted by \mathcal{E} is the set of all faces. Two subsets of interest are, the the set of boundary faces \mathcal{E}^∂ , and $\mathcal{E}^\circ = \mathcal{E} \setminus \mathcal{E}^\partial$ the set of interior faces.

Let $\mathbf{u}, \mathbf{v} : \mathbb{R}^d \rightarrow \mathbb{R}^m$ smooth vectorial functions with m components. For d -dimensional set $G \subset \mathbb{R}^d$ we define the inner products

$$\begin{aligned} (\mathbf{u}, \mathbf{v})_G &= \sum_{i=1}^m (\mathbf{u}_i, \mathbf{v}_i)_G \equiv \sum_{i=1}^m \int_G \mathbf{u}_i(\mathbf{x}) \mathbf{v}_i(\mathbf{x}) \, d\mathbf{x}. \\ \langle \mathbf{u}, \mathbf{v} \rangle_{\partial G} &= \sum_{i=1}^m \langle \mathbf{u}_i, \mathbf{v}_i \rangle_{\partial G} \equiv \sum_{i=1}^m \int_{\partial G} \mathbf{u}_i(\mathbf{x}) \mathbf{v}_i(\mathbf{x}) \, ds. \end{aligned}$$

For an element I , the latter reads

$$\langle \mathbf{u}, \mathbf{v} \rangle_{\partial I} = \sum_{e \in \partial I, e \in \mathcal{E}} \int_e \mathbf{u}_i(\mathbf{x}) \mathbf{v}_i(\mathbf{x}) \, ds.$$

Finally, we define $\mathcal{P}^p(I)$ the space of polynomials of degree less or equal than p on I , and $\mathbf{V}_m^p(I)$ the cartesian product of m -copies of $\mathcal{P}^p(I)$. Similarly, $\mathcal{P}^p(e)$ and $\mathbf{\Lambda}_m^p(e)$, for a face $e \in \mathcal{E}$.

2.1.2. First order hyperbolic system. Hereafter we use freely the theory of hyperbolic partial differential equations, see Leveque [10].

The first step is to reduce equation (1), to a first order hyperbolic system.

Let us introduce a variant of the reduction in Bui-Thanh [2]. We define the new variable (flux) $\mathbf{z} = -\mathbf{K}\nabla p$.

For clarity of exposition, we consider two dimensional problems.

Since the matrix \mathbf{K} is invertible, $\nabla p = -\mathbf{K}^{-1}\mathbf{z}$, we have the following system

$$\begin{aligned}\nabla p + \mathbf{K}^{-1}\mathbf{z} &= \mathbf{0} \\ \nabla \cdot \mathbf{z} - \beta \cdot \mathbf{K}^{-1}\mathbf{z} + cp &= f\end{aligned}$$

Set $\mathbf{z} = (z^1, z^2)$, $\beta = (\beta_1, \beta_2)$, and define

$$\mathbf{u} := \begin{pmatrix} z^1 \\ z^2 \\ p \end{pmatrix}, \mathbf{A}_1 := \begin{pmatrix} 0 & 0 & 1 \\ 0 & 0 & 0 \\ 1 & 0 & 0 \end{pmatrix}, \mathbf{A}_2 := \begin{pmatrix} 0 & 0 & 0 \\ 0 & 0 & 1 \\ 0 & 1 & 0 \end{pmatrix},$$

$$\mathbf{B} := \begin{pmatrix} k_1^{-1} & 0 & 0 \\ 0 & k_2^{-1} & 0 \\ -k_1^{-1}\beta_1 & -k_2^{-1}\beta_2 & c \end{pmatrix}, \mathbf{f} := \begin{pmatrix} 0 \\ 0 \\ f \end{pmatrix}.$$

The system becomes

$$(2) \quad \frac{\partial}{\partial x}(\mathbf{A}_1\mathbf{u}) + \frac{\partial}{\partial y}(\mathbf{A}_2\mathbf{u}) + \mathbf{B}\mathbf{u} = \mathbf{f}.$$

Let \mathbf{n} , be an arbitrary vector, and $\mathbf{A} := n_1\mathbf{A}_1 + n_2\mathbf{A}_2$. It is readily seen that

$$\mathbf{A} = \begin{pmatrix} 0 & 0 & n_1 \\ 0 & 0 & n_2 \\ n_1 & n_2 & 0 \end{pmatrix}$$

with real eigenvalues $\{0, \sqrt{n_1^2 + n_2^2}, -\sqrt{n_1^2 + n_2^2}\}$. Hence the matrix and the system are hyperbolic.

For later reference, let us write

$$\mathbf{A} = \mathbf{R}\mathbf{D}\mathbf{R}^{-1}, \quad |\mathbf{A}| := \mathbf{R}|\mathbf{D}|\mathbf{R}^{-1}$$

where $\mathbf{R} = [\mathbf{r}_1, \mathbf{r}_2, \mathbf{r}_3]$ is the matrix of eigenvectors,

$$\mathbf{D} = \text{diag}(0, -\sqrt{n_1^2 + n_2^2}, \sqrt{n_1^2 + n_2^2}) \equiv \text{diag}(\lambda_1, \lambda_2, \lambda_3),$$

and

$$|\mathbf{D}| := \text{diag}(|\lambda_1|, |\lambda_2|, |\lambda_3|).$$

Finally, for any matrix \mathbf{O} , we denote by \mathbf{O}_i , \mathbf{O}^j its row i , and column j respectively.

2.1.3. *Local DG formulation with Godunov flux.* Let us define

$$F_i(\mathbf{u}) := ((\mathbf{A}_1)_i \mathbf{u}, (\mathbf{A}_2)_i \mathbf{u}), \quad i = 1, 2, 3,$$

and

$$F(\mathbf{u}) := \begin{bmatrix} F_1(\mathbf{u}) \\ F_2(\mathbf{u}) \\ F_3(\mathbf{u}) \end{bmatrix}.$$

We apply operators component wise. For instance, for the divergence operator we have,

$$\nabla \cdot F(\mathbf{u}) := \begin{bmatrix} \nabla \cdot F_1(\mathbf{u}) \\ \nabla \cdot F_2(\mathbf{u}) \\ \nabla \cdot F_3(\mathbf{u}) \end{bmatrix}.$$

We can write the system (2) in the form

$$(3) \quad \nabla \cdot F(\mathbf{u}) + \mathbf{B}\mathbf{u} = \mathbf{f},$$

Compute the inner product on I of each side of (3) with a test function $\mathbf{v} \in \mathbf{V}_3^p(I)$, to obtain

$$(4) \quad (\nabla \cdot F(\mathbf{u}), \mathbf{v})_I + (\mathbf{B}\mathbf{u}, \mathbf{v})_I = (\mathbf{f}, \mathbf{v})_I.$$

Integrating by parts,

$$(5) \quad - (F(\mathbf{u}), \nabla \mathbf{v})_I + \langle F(\mathbf{u}) \cdot \mathbf{n}, \mathbf{v} \rangle_{\partial I} + (B\mathbf{u}, \mathbf{v})_I = (\mathbf{f}, \mathbf{v})_I,$$

Continuity is not enforced at the boundary of adjacent elements. Therefore, the boundary term $F(\mathbf{u})$ is replaced with a boundary numerical flux $F^*(u^-, u^+)$. As customary, the $-$ superscript denotes limits from the interior of I , and the $+$ superscript, limits from the exterior. In this context, element I is denoted by I^- and the outer normal \mathbf{n} by \mathbf{n}^- .

A classical numerical flux is that of Godunov given by

$$(6) \quad F^* \cdot \mathbf{n}^- := F(u^-) \cdot n^- + |\mathbf{A}|(u^- - u^*).$$

Here $u^* \equiv u^*(u^-, u^+)$ is the solution of a Riemann problem along the normal \mathbf{n}^- of I^- .

The Godunov flux for the adjacent element I^+ on the same face of the boundary ∂I^- is given by

$$(7) \quad F^* \cdot \mathbf{n}^+ := F(u^+) \cdot n^+ + |\mathbf{A}|(u^+ - u^*).$$

The following identity holds

$$F^* \cdot \mathbf{n}^- + F^* \cdot \mathbf{n}^+ = 0.$$

Or in terms of the the jump operator

$$\begin{aligned} \llbracket (\cdot) \rrbracket &= (\cdot)^- + (\cdot)^+, \\ \llbracket F(u) \cdot n + |\mathbf{A}|(u - u^*) \rrbracket &= 0. \end{aligned}$$

Combining adjacent fluxes

$$F^* \cdot \mathbf{n}^- = \frac{1}{2} [F(u^-) + F(u^+)] \cdot \mathbf{n}^- + \frac{1}{2} |\mathbf{A}|(u^- - u^+).$$

This is the symmetric form of the Godunov flux used in upwind DG. It couples the unknowns of the adjacent elements, and hence the unknowns of all elements.

2.1.4. *Hybrid flux.* Observe that the upwind fluxes (6), (7) depend on the DG unknowns of only one side of a face and the single-valued solution u^* of the Riemann problem. If u^* is given, the numerical flux is completely determined using only information from either side of the face. Moreover, we then can solve for u element-by-element independent of each other.

To hybridized the flux, and break the coupling, u^* is regarded as an extra unknown to be solved on the skeleton of the mesh instead of using the Riemann/upwind state which couples the local unknown u . Renaming u^* as \hat{u} and F^* as \hat{F} , we are led to

$$(8) \quad \hat{F} \cdot \mathbf{n} := F(u) \cdot \mathbf{n} + |\mathbf{A}|(u - \hat{u}).$$

This is the hybridized upwind flux or HDG flux.

In summary, for each element I , the DG local unknown u and the extra *trace* unknown \hat{u} need to satisfy

$$(9) \quad -(F(\mathbf{u}), \nabla \mathbf{v})_I + \langle \hat{F}(\mathbf{u}^-, \hat{u}) \cdot \mathbf{n}^-, \mathbf{v} \rangle_{\partial I} + (\mathbf{B}\mathbf{u}, \mathbf{v})_I = (\mathbf{f}, \mathbf{v})_I, \quad \mathbf{v} \in \mathbf{V}_3^p(I).$$

This is complemented with a weak jump condition in the skeleton. Namely, for all $e \in \mathcal{E}$,

$$(10) \quad \langle \llbracket \hat{F} \cdot \mathbf{n} \rrbracket, \mathbf{w} \rangle_e = 0, \quad \mathbf{w} \in \Lambda_m^p(e).$$

2.1.5. *The discrete problem.* Let us solve equation (9) for the \mathbf{u} terms, and (10) for the $\hat{\mathbf{u}}$ terms. We obtain,

$$(11) \quad -(F(\mathbf{u}), \nabla \mathbf{v})_I + \langle F(\mathbf{u}^-) \cdot \mathbf{n}^- + |\mathbf{A}|\mathbf{u}^-, \mathbf{v} \rangle_{\partial I} + (\mathbf{B}\mathbf{u}, \mathbf{v})_I = (\mathbf{f}, \mathbf{v})_I + \langle |\mathbf{A}|\hat{\mathbf{u}}, \mathbf{v} \rangle_{\partial I}.$$

$$(12) \quad \langle 2|\mathbf{A}|\hat{\mathbf{u}}, \mathbf{w} \rangle_e = \langle \llbracket F(\mathbf{u}) \cdot \mathbf{n} + |\mathbf{A}|\mathbf{u} \rrbracket, \mathbf{w} \rangle_e.$$

Let $\{\mathbf{N}_j : j = 1, \dots, P_I\}$ be a basis of $\mathbf{V}_3^p(I)$. Hence

$$\mathbf{u} = \sum_{j=1}^{P_I} \mathbf{u}_j \mathbf{N}_j$$

Since $F(\mathbf{u}) = \mathbf{A}_1 \mathbf{u} + \mathbf{A}_2 \mathbf{u}$ and $A = (n_I)_1 A_1 + (n_I)_2 A_2$, for $i = 1, \dots, P_I$, equation (11) reads

$$(13) \quad \sum_{j=1}^{P_I} [(-(\mathbf{A}_1 + \mathbf{A}_2)\mathbf{N}_j, \nabla \cdot \mathbf{N}_i)_I + (B\mathbf{N}_j, \mathbf{N}_i)_I + \langle (\mathbf{A} + |\mathbf{A}|)\mathbf{N}_j^-, \mathbf{N}_i^- \rangle_{\partial I}] \mathbf{u}_j \\ = (\mathbf{f}, \mathbf{N}_i)_I + \langle |\mathbf{A}|\hat{\mathbf{u}}, \mathbf{N}_i^- \rangle_{\partial I}$$

Similarly, let $\{\mathbf{M}_j : j = 1, \dots, Q_e\}$ be a basis of $\Lambda_3^p(e)$. For $i = 1, \dots, Q_e$, equation (12) reads

$$(14) \quad \sum_{j=1}^{Q_e} \langle 2|\mathbf{A}|\mathbf{M}_j, \mathbf{M}_i \rangle_e \hat{\mathbf{u}}_j = \langle \llbracket F(\mathbf{u}) \cdot \mathbf{n} + |\mathbf{A}|\mathbf{u} \rrbracket, \mathbf{w} \rangle_e.$$

Solving for \mathbf{u} on each element form (13) and substituting in the corresponding edges in equation (14), we are led to a sparse linear system for the hatted unknown on the skeleton.

Then one solves the small and independent linear systems (13) for the local variables on each element. The latter can be done in parallel.

2.1.6. Element basis functions. The DG method is H^p adaptative, it is straightforward to make the order of approximation element dependent. The method is also suitable for irregular geometries and unstructured meshes. Nevertheless, we do not aim for generality. We shall test on benchmark problems in rectangular geometries and regular meshes.

For one dimensional problems we use second order nodal functions on the reference interval $[-1, 1]$,

$$N_0(\xi) = \frac{\xi^2 - \xi}{2}, \quad N_1(\xi) = 1 - \xi^2, \quad N_2(\xi) = \frac{\xi^2 + \xi}{2}.$$

An easy 2D extension is achieved by considering the basis functions

$$N_{ij}(\xi, \zeta) = N_i(\xi) N_j(\zeta), \quad i, j = 0, 1, 2,$$

defined on the reference square $[-1, 1] \times [-1, 1]$.

This basis will help to illustrate the performance of a high order DG method.

2.2. A pressure projection method with HDG Poisson solver. Pressure projection methods are well known, a thorough study is presented in Almgren et al [1]. As a primer, we introduce a PP method in a pressure splitting framework to be applied in 2D vertical-slice modeling. Our purpose is to stress the use of the HDG solver of the underlying Poisson problem.

Let us consider unsteady, constant density, incompressible flow. Let ρ_0 be the reference density. The flow is governed by the momentum and continuity equations

$$\begin{aligned} \frac{\partial \mathbf{u}}{\partial t} &= -\frac{1}{\rho_0} \nabla P - (\mathbf{u} \cdot \nabla) \mathbf{u}, \\ \nabla \cdot \mathbf{u} &= 0. \end{aligned}$$

Let Δt be the time step. Assume the velocity \mathbf{u}^n and pressure P^n are given at time t_n .

Split pressure P^{n+1} in the form

$$P^{n+1} = p^n + q^{n+1}$$

where p^n , q^{n+1} are hydrostatic and non hydrostatic pressure respectively. The latter is of the form

$$q^{n+1} = q^n + \delta q^{n+1}.$$

The non hydrostatic correction δq^{n+1} is to be determined.

The main steps are:

Step 1. Construct an intermediate velocity $\mathbf{u}^{n+1/2}$ by advancing the momentum equations,

$$\mathbf{u}^{n+1/2} = \mathbf{u}^n - \frac{\Delta t}{\rho_0} \nabla P^n - (\mathbf{u}^n \cdot \nabla) \mathbf{u}^n$$

Step 2. Pressure correction. For suitable boundary conditions, HDG solve the Poisson equation

$$-\Delta(\delta q^{n+1}) = -\frac{\rho_0}{\Delta t} \nabla \cdot \mathbf{u}^{n+1/2}.$$

Step 3. Update the divergence free velocity field,

$$\mathbf{u}^{n+1} = \mathbf{u}^{n+1/2} - \frac{\rho_0}{\Delta t} \nabla(\delta q^{n+1}).$$

It is straightforward to modify this scheme for more general unsteady equations. We show some examples below.

3. TIDAL SIMULATION IN SEMIENCLOSED BASIN

We consider two benchmark problems that lead to elliptic equations. A comparison is made with the solution of FVCOM as presented in Chen et al [3]. Therein, FVCOM is applied for modeling of tidal simulation in semienclosed basin with tidal forcing at the open boundary under nonresonance and near resonance conditions. Here we apply HDG to illustrate the accurate simulation of the troublesome near resonance case.

3.1. A Rectangular Channel. Consider a fluid layer of uniform density that propagates along a channel aligned with the x -direction. More precisely, a semienclosed narrow channel with length L and variable depth $H(x)$ and a closed boundary at $x = L_1$ and an Open Boundary at $x = L$.

Neglecting Coriolis force and advection of momentum, the governing equations modeling tidal waves propagation in the semienclosed channel (see Figure 1) are given as

$$\frac{\partial u}{\partial t} + g \frac{\partial \zeta}{\partial x} = 0; \quad \frac{\partial \zeta}{\partial t} + g \frac{\partial u H}{\partial x} = 0; \quad (x, t) \in (a, b) \times (0, T).$$

Here, $H(x)$ is the total water depth, g is acceleration due to gravity, u is speed in the x -direction, and ζ is sea-level elevation .

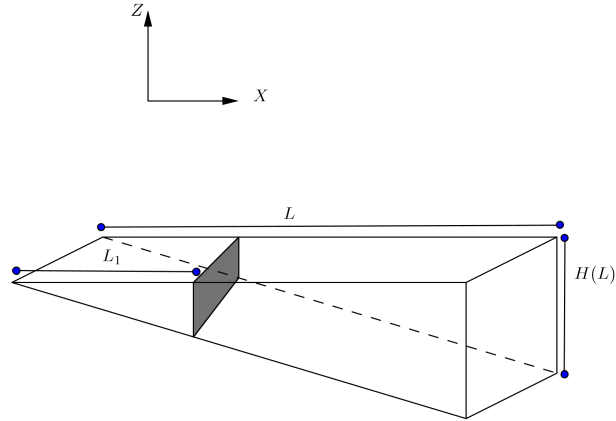


FIGURE 1. Configuration of the semienclosed channel.

Assuming harmonic solutions,

$$\zeta = \zeta_0(x)e^{-i\sigma t}, \quad u = u_0(x)e^{-i\sigma t},$$

we obtain the ordinary second order equation for ζ_0

$$(15) \quad (H\zeta_0')' + \frac{\sigma^2}{g}\zeta_0 = 0.$$

We specify a periodic tidal forcing with amplitude A at the mouth of the channel,

$$\zeta_0(L) = A,$$

and a no-flux boundary condition at the wall,

$$H(L_1)\zeta_0'(L_1) = 0.$$

Let the water depth decrease linearly toward the end of the channel, so that $H(x)$ can be written as

$$H(x) = \frac{xH(L)}{L}.$$

It is readily seen that (15) is a Bessel's equation. With the given boundary conditions, the analytic solution is given by

$$\zeta_0(x) = A \frac{Y_0'(2k\sqrt{L_1})J_0(2k\sqrt{x}) - J_0'(2k\sqrt{L_1})Y_0(2k\sqrt{x})}{Y_0'(2k\sqrt{L_1})J_0(2k\sqrt{L}) - J_0'(2k\sqrt{L_1})Y_0(2k\sqrt{L})}$$

where

$$k := \frac{\sigma\sqrt{L}}{\sqrt{gH(L)}},$$

J_0, Y_0 are the Bessel's functions the degree zero and one respectively.

Elements	$\mathcal{E}_2(\text{HDG}_2)$	$\mathcal{E}_2(\text{FV})$
10	0.180784	22.3052
20	0.0748017	0.585413
40	0.0235224	0.553751
80	0.00684013	0.43336
160	0.00187985	0.297118
320	0.000495726	0.181964
640	0.000127432	0.102475
1280	0.0000324	0.0546902

TABLE 1. Relative root mean square error for HDG₂ and FV.

To compare with the HDG approximation, we solve the hyperbolic system,

$$\begin{aligned}\zeta_0' + H^{-1}z &= 0 \\ z' - \frac{\sigma^2}{g}\zeta_0 &= 0.\end{aligned}$$

Here $z = -H\zeta_0'$, (15).

The following parameters are considered for a channel very close to resonance.

$$L = 300km, L_1 = 10km, H(L) = 20.1m, \sigma = \frac{2\pi}{12.42 \cdot 3600s}, A = 1cm.$$

The HDG method is applied using nodal polynomials of degree 2 (HDG₂). It is compared with the FV method and the analytic solution. For consistency with the FV method, we consider the approximation at the middle point x_i of the element $I_i = [x_{i-\frac{1}{2}}, x_{i+\frac{1}{2}}]$. We compute the relative root mean square error for ζ_0^R the analytic solution and ζ_0 the numerical solution. Namely,

$$\mathcal{E}_2 := \frac{\|\zeta_0 - \zeta_0^R\|_2}{\|\zeta_0^R\|_2}.$$

As illustrated in Table 3.1, a second order approximation with HDG in a coarse resolution, is of greater quality than FV.

The analytic solution describes a standing wave with a node point near the closed side of the channel. As expected, the reproduction of these features by HDG is accurate. See Figure 2

Remark. As pointed out in Chen et al [3], regardless of the numerical method, a proper selection of horizontal resolution recover accurately this tidal resonance problem. We argue that the accuracy attained by HDG in coarse meshes yields a better choice.

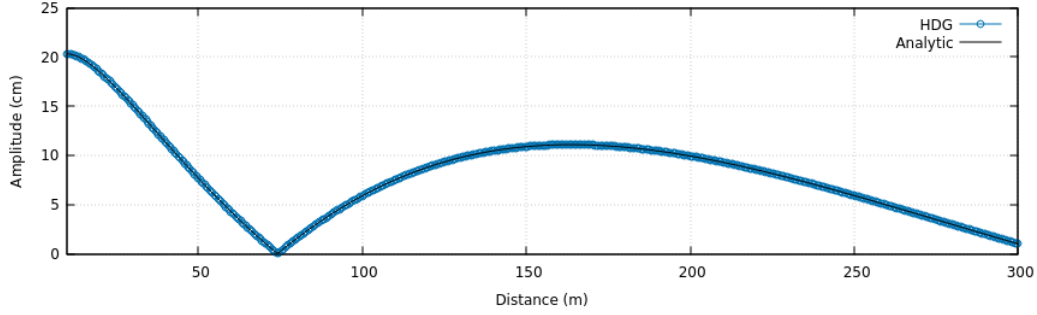


FIGURE 2. Solution for the rectangular channel near resonance case, with HDG nodal with polynomials of degree 2 and 80 elements.

3.2. A Sector Channel. Now consider a flat bottom channel in the form of a semicircular section, which in polar coordinates is defined from 0 to L in the radial direction and from $\alpha/2$ to $-\alpha/2$ in the angular direction.

The semicircular line of radius L corresponds to an open border, while along the semicircular line of radius L_1 and the two sides, they are closed, (Figure 3).

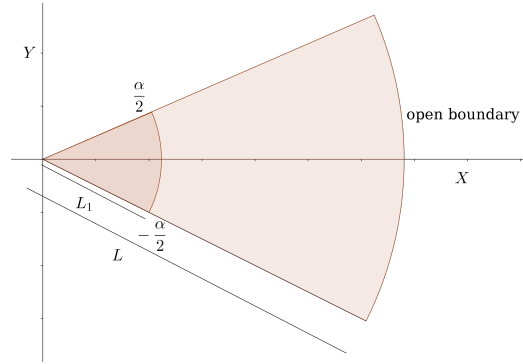


FIGURE 3. Semienclosed sector channel in the polar region $L_1 \leq r \leq L$, $-\frac{\alpha}{2} \leq \theta \leq \frac{\alpha}{2}$. The sector is open at $r = L$ and closed elsewhere.

The following equations govern the non rotating tidal oscillation,

$$(16) \quad \frac{\partial V_r}{\partial t} = -g \frac{\partial \eta}{\partial r},$$

$$(17) \quad \frac{\partial V_\theta}{\partial t} = -g \frac{\partial \eta}{r \partial \theta},$$

$$(18) \quad \frac{\partial \eta}{\partial t} + \frac{\partial r V_r H_0}{r \partial r} + \frac{\partial V_\theta H_0}{r \partial \theta} = 0.$$

H_0 is the constant water depth, V_r, V_θ are the radial and angular r, θ velocity components, and η is the free surface water elevation.

Assuming a harmonic solution,

$$\eta = \text{Re}(\eta_0(r, \theta)e^{-it(\omega t - \frac{\pi}{2})}),$$

we can reduce the equations (16-18) to an elliptic equation

$$(19) \quad \frac{\partial^2 \eta_0}{\partial r^2} + \frac{1}{r} \frac{\partial \eta_0}{\partial r} + \frac{1}{r^2} \frac{\partial^2 \eta_0}{\partial \theta^2} + \frac{\omega^2}{gH_0} \eta_0 = 0.$$

The physical boundary conditions are as follows

(1) At the open mouth of the channel, a harmonic tidal forcing is assumed,

$$\eta_0(r, \theta) = \bar{A} \cos\left(m\pi \frac{\theta + \frac{\alpha}{2}}{\alpha}\right), \quad \{L\} \times \left(-\frac{\alpha}{2}, \frac{\alpha}{2}\right),$$

(2) On the solid walls, null flux is prescribed,

$$-K \nabla \eta_0(r, \theta) = 0, \quad \{L_1\} \times \left(-\frac{\alpha}{2}, \frac{\alpha}{2}\right) \cup (L_1, L) \times \left\{-\frac{\alpha}{2}\right\} \cup (L_1, L) \times \left\{\frac{\alpha}{2}\right\}.$$

The analytic solution of this boundary-value problem is:

$$\eta_0(r, \theta) = \bar{A} \frac{Y'_v(L_1 \kappa) J_v(r \kappa) - J'_v(L_1 \kappa) Y_v(r \kappa)}{Y'_v(L_1 \kappa) J_v(L \kappa) - J'_v(L_1 \kappa) Y_v(L \kappa)} \cos\left(\frac{m\pi}{\alpha} \left(\theta + \frac{\alpha}{2}\right)\right)$$

where

$$v = \frac{m\pi}{\alpha}, \quad \kappa = \frac{\omega}{\sqrt{gH_0}},$$

J_v, Y_v are respectively the v th-order Bessel function of the first and second type.

Let us show the HDG solution in the rectangular domain $(L_1, L] \times (-\alpha/2, \alpha/2)$.

Let ∇ denote the gradient with respect to (r, θ) and let

$$K := \begin{pmatrix} 1 & 0 \\ 0 & \frac{1}{r^2} \end{pmatrix}.$$

Equation (19) becomes the diffusion-advection-reaction equation,

$$(20) \quad -\nabla \cdot (K \nabla \eta_0) - (r^{-1}, 0) \cdot \nabla \eta_0 - \frac{\omega^2}{gH_0} \eta_0 = 0.$$

We apply the fourth order (HDG₄) scheme developed above for a near resonance case. The geometric parameter values are:

$$H_0 = 1m, \quad \alpha = \frac{\pi}{4}, \quad L_1 = 90km, \quad m = 1.0, \quad \omega = \frac{2\pi}{12.42 \cdot 3600} \frac{1}{s}, \quad L = 158km, \quad \bar{A} = 1cm.$$

In Figure (4) the analytic and numerical solution are compared. The relative mean square error is shown in Table 2.

Remark. Noteworthy, the 10×10 HDG₄ solution is of grater quality that the 40×40 FV solution. On regards to execution time, the former is attained in half

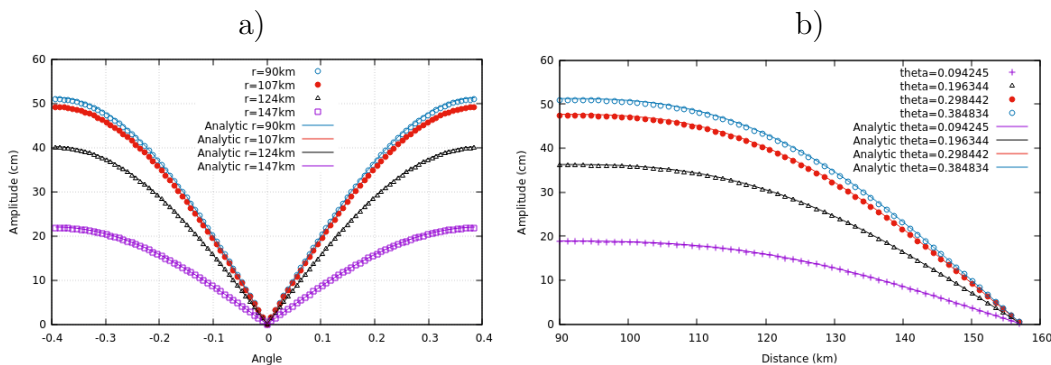


FIGURE 4. Comparison between the analytic solution to the sector problem with the HDG₄ solution using 30×50 elements. a) Solution for some r values, b) Solution for some θ values.

Elements	$\mathcal{E}_2(\text{HDG}_4)$	$\mathcal{E}_2(\text{FV})$
5×5	0.441213	0.920939
10×10	0.009879	0.887757
35×35	0.0026408	0.803039
40×40	0.00115041	0.794262

TABLE 2. Relative root mean square error for HDG₄ and FV.

a second in a personal laptop. A solution of the same quality would require in the order of minutes with the Finite Volume Method in a much finer mesh.

4. VERTICAL OCEAN-SLICE NONHYDROSTATIC MODELS

Our proposal is to use a high order HDG Poisson solver to accelerate pressure projection numerical methods. As a primer, we solve two simple unsteady problems in Coastal Ocean Modeling.

Let us consider the ocean as a vertical slice. As customary, flow and gradients of variables normal to this plane are assumed to vanish, and the Coriolis force is ignored. We address deep-water (short) surface gravity waves and density-driven currents.

Modeling is considered in the Cartesian coordinate system, in which x, y denote the horizontal coordinates, the slice is along the x -axis. Changes are constant on y -cross sections, all the normal forces to this slice are neglected. The vertical axis z points upward to the undisturbed surface water located at $z = 0$, η is the free surface water, h_0 is the undisturbed water depth, and h the total depth.

Assuming a flat bottom, the time space domain of interest is $\Omega_T = [0, T_f] \times [L_a, L_b] \times [-h_0, 0]$. For simulation, a uniform rectangular mesh is considered with $\Delta x \times \Delta z$ elements.

4.1. Surface Standing Waves in a Deep Basin. The benchmark that follows is solved with a non hydrostatic version of FVCOM in Lai et al [8]. It was selected to test the stability and accuracy of the split mode explicit non hydrostatic algorithm and the non hydrostatic pressure Poisson solver. The surface boundary condition requires an approximate treatment. Our pressure projection method with HDG Poisson solver is developed as an alternative.

Consider the governing equations for a standing wave under linear, inviscid, non rotating conditions,

$$\begin{aligned}\frac{\partial u}{\partial t} &= \frac{-1}{\rho_0} \frac{\partial P}{\partial x}, \\ \frac{\partial w}{\partial t} &= \frac{-1}{\rho_0} \frac{\partial P}{\partial z}, \\ \frac{\partial u}{\partial x} + \frac{\partial w}{\partial z} &= 0.\end{aligned}$$

Here, u, w are the velocities in direction x and z respectively, P is the dynamic pressure

$$P = p + q,$$

p the hydrostatic and q the non hydrostatic pressure. ρ_0 is the mean density. The latter equation simplifies to $P = q$.

The free surface water, η , is given by the volume-conservation,

$$(21) \quad \frac{\partial \eta}{\partial t} = -\frac{\partial}{\partial x}(h \langle u \rangle); \quad \langle u \rangle(x) := \frac{1}{h} \int_{z_0}^{z_0+h} u(t, x, z) dz.$$

To relate the sea level elevation with the non hydrostatic dynamic pressure, the hydrostatic approximation is used,

$$(22) \quad q_s = \rho_0 g \eta \implies \frac{\partial q_s}{\partial t} = -\rho_0 g \frac{\partial}{\partial x}(h \langle u \rangle).$$

Here, $g := 9.81 \frac{m}{s^2}$.

Hence, the full set of equations are,

$$(23) \quad \frac{\partial u}{\partial t} = \frac{-1}{\rho_0} \frac{\partial q}{\partial x},$$

$$(24) \quad \frac{\partial w}{\partial t} = \frac{-1}{\rho_0} \frac{\partial q}{\partial z},$$

$$(25) \quad \frac{\partial u}{\partial x} + \frac{\partial w}{\partial z} = 0,$$

$$(26) \quad \frac{\partial q_s}{\partial t} = -\rho_0 g \frac{\partial}{\partial x}(h \langle u \rangle).$$

4.1.1. *Pressure splitting.* Here we apply the PP method to the velocity field

$$\mathbf{u} = \begin{pmatrix} u \\ w \end{pmatrix}.$$

It is left to update the correction pressure at the surface δq_s^{n+1} .

The approximation is made using the fact that

$$q_s^{n+1} = q_s^n + \delta p_s^{n+1} \implies \delta q_s^{n+1} = q_s^{n+1} - q_s^n.$$

It follows at once that

$$\begin{aligned} \delta q_s^{n+1} &= \Delta t \frac{q_s^{n+1} - q_s^n}{\Delta t} \\ &\approx \Delta t \frac{\partial q_s^n}{\partial t} \\ &= -\Delta t \rho_0 g \frac{\partial}{\partial x} (h < u^n >). \end{aligned}$$

Approximating the derivative with respect to x we have

$$(27) \quad \delta q_s^{n+1} = -\frac{\Delta t}{\Delta x} \rho_0 g \left[\int_{-h_0}^{\eta^n} u(t^n, x_k, z) dz - \int_{-h_0}^{\eta^n} u(t^n, x_{k-1}, z) dz \right].$$

The following numerical results was solved the HDG with nodal polynomials of degree $\vartheta = 2$.

4.1.2. *A test example.* Lai et al. [8] run FVCOM in a closed rectangular channel $L = 10$ meters long and $H = 10$ meters deep.

The initial condition are,

$$\begin{aligned} u(0, x, z) &= 0, \\ w(0, x, z) &= 0, \\ q(0, x, z) &= \rho_0 g \eta_0 \frac{\cosh(\kappa(-z + H))}{\cosh(\kappa H)} \cos(\kappa x). \end{aligned}$$

For the next time steps, we set for the Poisson equation

$$q(t > 0, x, 0) = \rho_0 g \frac{\cosh(\kappa(H))}{\cosh(\kappa H)} \eta(x),$$

$$\nabla q(t > 0, x, z > 0) \cdot \vec{\mathbf{n}} = 0, \quad ,$$

where $\rho_0 = 1000 \text{ Kg/m}^3$. A unimodal standing wave of free surface perturbation is considered, that is,

$$\eta(x) = \eta_0 \cos(\kappa x) \cos(\omega t).$$

The analytical solution of this problem can be found for instance in Jankowski [5]. It is a non hydrostatic deep water wave with phase speed $\omega = \sqrt{g \kappa \tanh(\kappa H)}$.

In Lai et al. [8] a non overlapping unstructured triangular grid is created by dividing each square into two triangles, with a triangle's side length of 0.25 m.

Consequently we work with a square mesh with $dx = dz = 0.25$. In our simulation $\kappa = \frac{\pi}{L} = \frac{\pi}{10}$; $\eta_0 = 0.1$ small enough so that $\frac{\eta_0}{H} \ll 1$.

As in Lai et al. [8] to test the stability of the program, it is run for 10 minutes. Therein the time step is $0.05s$, the high order used in HDG allows a larger step, $dt = 0.5s$.

In Figure (5) we show some snapshots of pressure, scaled to $[-1, 1]$.

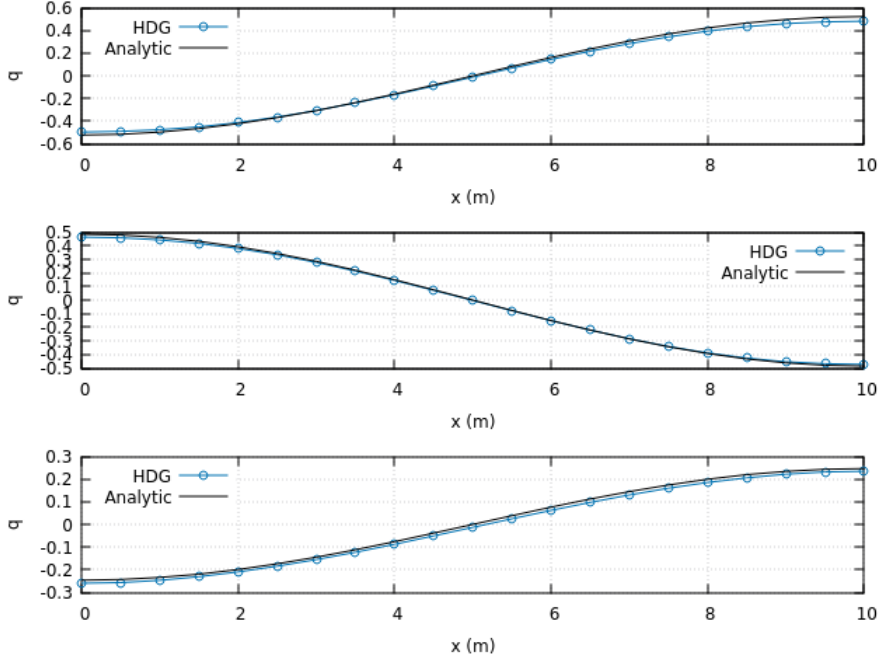


FIGURE 5. Comparison between the HDG and analytic solutions of pressure at a depth of $z = 1$ meters for $t = 2, 4, 10$ minutes respectively.

4.2. Density driven flow. Now we consider density effects in the vertical ocean-slice model by adding an advection-diffusion equation for density and the reduced-gravity force in the vertical momentum equation. The governing equations can be

written as:

$$(28) \quad \frac{\partial u}{\partial t} = -\frac{1}{\rho_0} \frac{\partial P}{\partial x} - (u, w) \cdot \nabla u,$$

$$(29) \quad \frac{\partial w}{\partial t} = -\frac{1}{\rho_0} \frac{\partial P}{\partial z} - \frac{\rho - \rho_0}{\rho_0} g - (u, w) \cdot \nabla w,$$

$$(30) \quad \frac{\partial \rho}{\partial t} = \nabla \cdot \left(\begin{pmatrix} K_h & 0 \\ 0 & K_z \end{pmatrix} \nabla \rho \right) - (u, w) \cdot \nabla \rho,$$

$$(31) \quad \nabla \cdot (u, w) = 0,$$

$$(32) \quad P_s = -\rho_0 g \frac{\partial}{\partial x} (h < u >).$$

Splitting the pressure in to hydrostatic and non hydrostatic pressure respectively,

$$P = p + q,$$

and using the hydrostatic approximation

$$-\frac{1}{\rho_0} \frac{\partial p}{\partial z} - \frac{\rho - \rho_0}{\rho_0} g = 0$$

The set of equations (28-32) can be written as

$$(33) \quad \frac{\partial u}{\partial t} = -\frac{1}{\rho_0} \frac{\partial (p + q)}{\partial x} - (u, w) \cdot \nabla u,$$

$$(34) \quad \frac{\partial w}{\partial t} = -\frac{1}{\rho_0} \frac{\partial q}{\partial z} - (u, w) \cdot \nabla w,$$

$$(35) \quad \frac{\partial \rho}{\partial t} = \nabla \cdot \left(\begin{pmatrix} K_h & 0 \\ 0 & K_z \end{pmatrix} \nabla \rho \right) - (u, w) \cdot \nabla \rho,$$

$$(36) \quad \nabla \cdot (u, w) = 0,$$

$$(37) \quad P_s = -\rho_0 g \frac{\partial}{\partial x} (h < u >),$$

$$(38) \quad \frac{\partial p}{\partial z} = -(\bar{\rho} - \rho_0)g, p(z = 0) = 0.$$

Vertical elements are indexed by i . Thus, we have $\bar{\rho} := 0.5(\rho_{i-1} + \rho_i)$ in element i .

4.2.1. *Pressure splitting.* To solve the last set of equation, we apply again pressure splitting. To complete the scheme, water's density is updated by a simple finite difference,

$$\rho^{n+1} = \rho^n + \Delta t \nabla \cdot \left(\begin{pmatrix} K_h & 0 \\ 0 & K_z \end{pmatrix} \nabla \rho^n \right) - \Delta t (u^n, w^n) \cdot \nabla \rho^n.$$

whereas the hydrostatic pressure

$$\frac{\partial p}{\partial z} = -(\bar{\rho} - \rho_0)g, p(z = 0) = 0, \bar{p} := 0.5(p_{i-1} + p_i)$$

4.2.2. *A density driven flow with variable bottom topography.* As a final example, let us consider a closed channel problem solved by Finite Differences in Kämpf [6]. The closed channel is initially composed of two vertical layers of water with constant but distinct density. The model is forced via prescription of a layer of dense water that initially leans against the left boundary. The variable bottom topography includes a ramp and a vertical bar, see Figure 6.

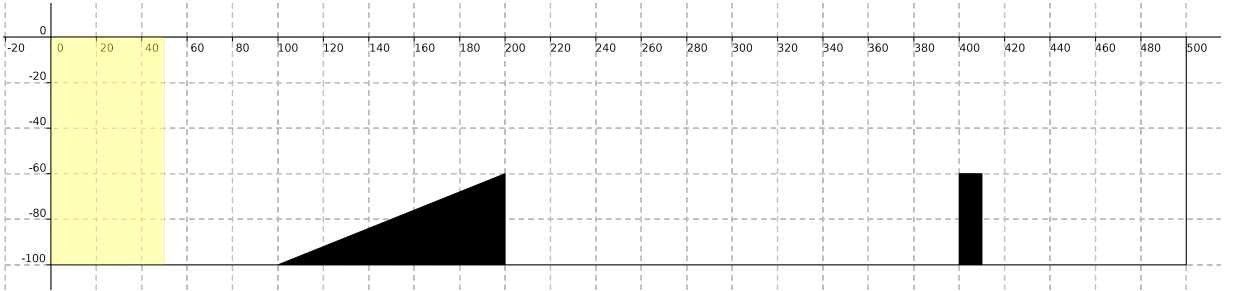


FIGURE 6. Bathymetry for the variable density problem. The left rectangular (yellow color) is a column of water with density $1029kg/m^3$, the triangle and the right rectangular (both in black color) are part of the sea floor. The remain domain is water with density $1028kg/m^3$.

The closed channel occupies the rectangle $\Omega = [0, 500] \times [-100, 0]$. The reference density is given by $\rho_0 = 1028kg/m^3$, and a column of water with density $\rho_1 = 1029kg/m^3$ is included in the region $\Omega_1 = [0, 50] \times [-100, 0]$. The system starts at rest.

For the horizontal and vertical density diffusivities we set $K_h = K_z = 10^{-4}m^2/s$. As in Kämpf [6], for the mesh we use the grid spacing of $\Delta x = 5m$, $\Delta z = 2m$, and a time step $\Delta = 0.1s$.

Numerical solutions are presented in the figure (7). Therein, a comparison of the solution obtained with the HDG_4 scheme is compared with the second order finite difference method (FD2) in in Kämpf [6].

We also solve the problem with a second order Discontinuous Galerkin method, HDG_2 . The approximation is comparable to FD2, this is illustrated in table 3, using the HDG_4 as the true solution. The graphical comparison in figure 8.

5. CONCLUSIONS

We have proposed a Hybrid Discontinuous Galerkin method for solutions of elliptic problems. It reduces the number of coupled unknowns arising from the classical Discontinuous Galerkin Method. Moreover, it does not require penalization terms as typical DG solutions of elliptic problems. A high order implementation provides fast and robust solutions.

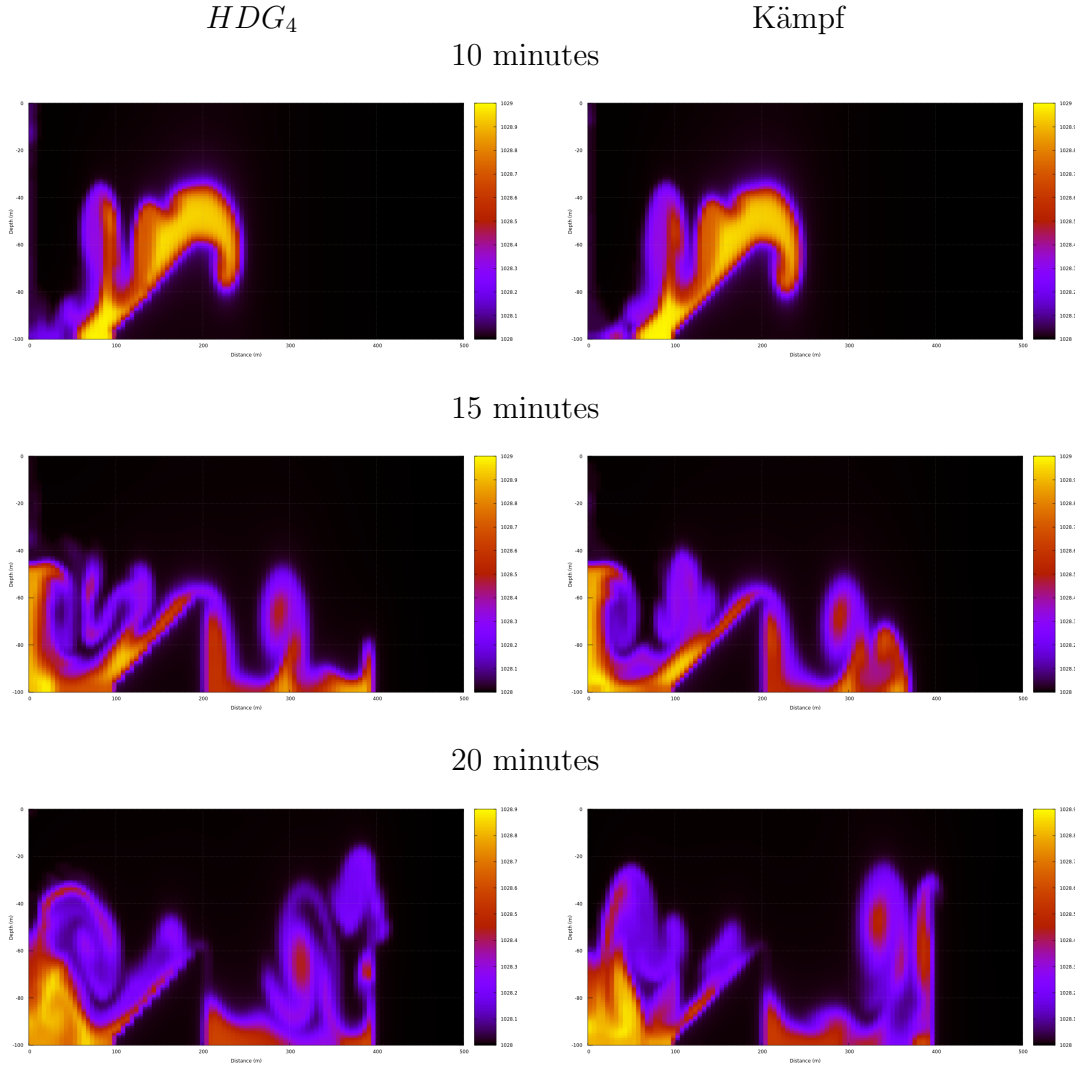


FIGURE 7. Comparison of the numerical solution of HDG_4 and the FD2 algorithm for the variable density problem.

Time (min)	$\mathcal{E}_2(HDG_2)$	$\mathcal{E}_2(\text{Kämpf's})$
7	6.55×10^{-5}	6.77×10^{-5}
9	0.00010759	0.000107866
13	0.000104016	0.000107906

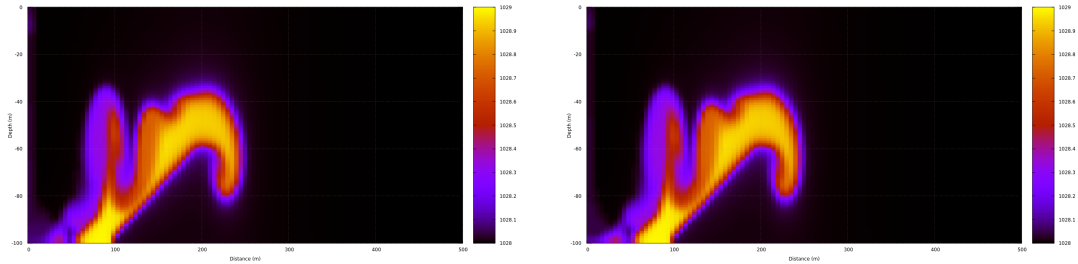
TABLE 3. Comparison of the HDG_2 and Kämpf algorithms for the variable density problem taking the HDG_4 as reference.

These features are illustrated on elliptic problems arising from Coastal Ocean Modeling. Even in the sector channel problem involving an advection term, results are highly satisfactory.

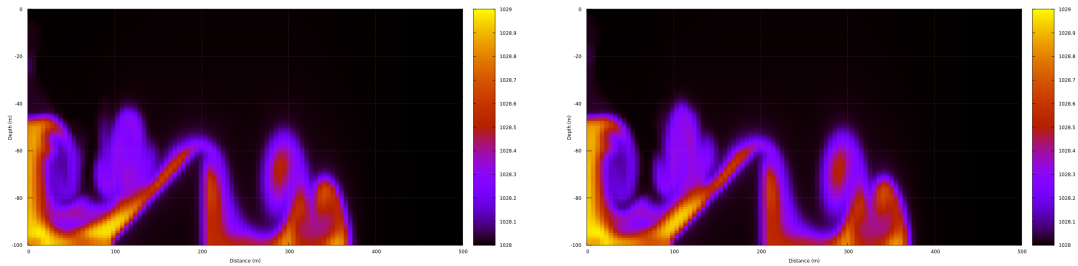
HDG_2

Kämpf

10 minutes



15 minutes



20 minutes

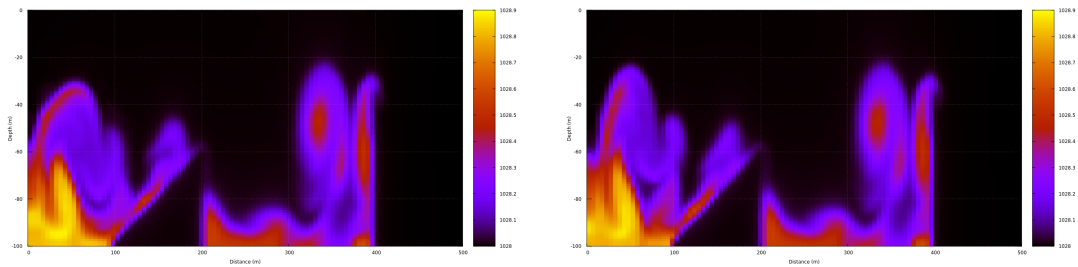


FIGURE 8. Comparison of the numerical solution of HDG_2 and the Kämpf's algorithm for the variable density problem.

In a pressure projection method for unsteady Navier-Stokes equations, the HDG elliptic solver can be used to solve the Poisson problems in each time step. Thus accelerating computations. As a primer we have considered two slice non hydrostatic problems from the literature. It is shown that straightforward modifications for the pressure correction method, yield accurate solutions.

We stress that the simplest grids and time advancing schemes have been used. The extension to more sophisticated situations is straightforward.

Of current and future interest, is to apply this HDG approach to more sophisticated unsteady problems. We shall report on this elsewhere.

REFERENCES

- [1] Almgren, A. S., Bell, J. B., & Crutchfield, W. Y. (2000). Approximate projection methods: Part I. Inviscid analysis. *SIAM Journal on Scientific Computing*, 22(4), 1139-1159.
- [2] T. Bui-Thanh. From Godunov to a unified hybridized discontinuous Galerkin framework for partial differential equations. *Journal of Computational Physics*, 295, 114 - 146. (2015)
- [3] Chen, C., Huang, H., Beardsley, R. C., Liu, H., Xu, Q., & Cowles, G. (2007). A finite volume numerical approach for coastal ocean circulation studies: Comparisons with finite difference models. *Journal of Geophysical Research: Oceans*, 112(C3).
- [4] A. Ern, J. L. Guermond: Discontinuous Galerkin methods for Friedrichs' systems. Part II. second-order elliptic PDEs. *SIAM Journal on Numerical Analysis*, 44(6), 2363 - 2388. (2006)
- [5] Jankowski, J. A. (1999), A nonhydrostatic model for free surface flows, Ph.D. dissertation, 251 pp., Univ. of Hannover, Germany.
- [6] J. Kämpf: Advanced ocean modelling: using open-source software. Springer Science & Business Media, 2010.
- [7] Kärnä, T., Kramer, S. C., Mitchell, L., Ham, D. A., Piggott, M. D., & Baptista, A. M. (2018). Thetis coastal ocean model: discontinuous Galerkin discretization for the three-dimensional hydrostatic equations. *Geoscientific Model Development*, 11(11), 4359 - 4382.
- [8] Lai, Z., Chen, C., Cowles, G. W., & Beardsley, R. C. (2010). A nonhydrostatic version of FVCOM: 1. Validation experiments. *Journal of Geophysical Research: Oceans*, 115(C11).
- [9] Pan, W., Kramer, S. C., Kärnä, T., & Piggott, M. D. (2020). Comparing non-hydrostatic extensions to a discontinuous finite element coastal ocean model. *Ocean Modelling*, 101634.
- [10] Randall J. Leveque. Finite-Volume methods for hyperbolic problems. Cambridge texts in applied mathematics. (2004).
- [11] Riviere, B. (2008). Discontinuous Galerkin methods for solving elliptic and parabolic equations: theory and implementation. Society for Industrial and Applied Mathematics.

D. AZOFEIFA, M. A. MORELES, CENTRO DE INVESTIGACIÓN EN MATEMÁTICAS, JALISCO S/N, VALENCIANA, GUANAJUATO, GTO 36240, MEXICO, *Email address*, MORELES@CIMAT.MX: ,
 F. VELAZQUEZ, DEPARTMENT OF PHYSICS, UNIVERSITY OF GUADALAJARA, GUADALAJARA 44100, MEXICO